JOURNAL OF SPACECRAFT AND ROCKETS
Vol. 39, No. 4, July–August 2002

Thermal Analysis and Design Optimization of Multilayer Insulation for Reentry Aerodynamic Heating

Kamran Daryabeigi*
NASA Langley Research Center, Hampton, Virginia 23681

A design-of-experiment technique was used to investigate optimum design of multilayer insulations for reentry aerodynamic heating. Combined radiation/conduction heat transfer in high-temperature multilayer insulations was modeled using a finite volume numerical model, which was validated by comparison with steady-state effective thermal conductivity measurements, and transient thermal tests simulating reentry aerodynamic heating conditions. It was found that use of 2-mm foil spacing and locating the foils near the hot boundary, with the top foil 2 mm away from the hot boundary, resulted in the most effective insulation design. A 76.2-mm-thick multilayer insulation using 1, 4, or 16 foils resulted in 2.9, 7.2, or 22.2% mass per unit area savings, respectively, compared to a fibrous insulation sample at the same thickness.

Nomenclature

c = specific heat, J/kg/K
D_f = fiber diameter, m
d_g = gas collision diameter, m
e = specific extinction coefficient ($e = \beta/\rho$), m^2/kg
f = solid fraction ratio
G = incident radiation energy per unit area, W/m^2
K_B = Boltzmann constant, 1.3806×10^{-23} J/K
k = thermal conductivity, W/m/K
L = overall insulation thickness, m
L' = fibrous insulation spacer thickness, m
L_c = characteristic length, m
P = pressure, Pa
Pr = Prandtl number
q'' = heat flux, W/m^2
T = temperature, K
t = time, s
x = spatial coordinate, m
α = thermal accommodation coefficient
β = extinction coefficient, 1/m
γ = specific heat ratio
ε = emittance
λ_m = molecular mean free path, m
ρ = density, kg/m^3
σ = Stefan–Boltzmann constant, 5.668×10^{-8} W/m^2/K^4
τ_o = optical thickness
ω = albedo of scattering

Subscripts

g = gas
r = radiation
s = solid

Superscripts

$*$ = property at atmospheric pressure
$**$ = property of parent material

Received 4 October 2001; revision received 14 March 2002; accepted for publication 23 March 2002.

*Aerospace Engineer, Metals and Thermal Structures Branch, Mail Stop 396. Senior Member AIAA.

Introduction

A THERMAL protection system is used to maintain a reusable launch vehicle's structural temperature within acceptable limits during reentry flight. Metallic thermal protection systems have been considered for reusable launch vehicles.[1] A metallic thermal protection system consists of a metallic shell panel fabricated from a high-temperature metallic alloy and mechanically attached to the vehicle structure; the shell is filled with lightweight, non-load-bearing fibrous insulation. The use and optimization of high-temperature multilayer insulation for metallic thermal protection systems is investigated in the present study. The multilayer insulation considered consists of thin ceramic foils with high reflectance gold coatings separated by fibrous insulation spacers.

Heat transfer through a multilayer insulation during atmospheric reentry involves combined modes of heat transfer: solid conduction through fibers, gas conduction in spaces between fibers, and radiation interchange through participating media in the fibrous insulation spacers between reflective foils. The objective of this investigation was to model the combined radiation/conduction heat transfer through multilayer insulation with a numerical model validated by experimental tests and to use the numerical model to design optimum multilayer configurations.

In the present work the effective thermal conductivity of a multilayer insulation was measured over an extended temperature and pressure range, 373–1273 K and 1.33×10^{-5}–101.32 kPa. Furthermore, transient tests simulating reentry aerodynamic heating conditions were performed in a thermal vacuum chamber. The heat transfer through the insulation was modeled using combined solid and gaseous conduction and radiation. The radiation heat transfer was modeled using the two-flux approximation, which is valid over various optical thicknesses and is not limited to the optically thin or optically thick approximations. The governing conservation of energy equation was modeled using the finite volume technique, and the governing incident radiation equations were modeled using the finite difference approximation. The numerical heat-transfer model was validated by comparison with both steady-state and transient measurements. The validated model was then used to design optimum multilayer configurations for typical reentry aerodynamic heating loads using a design-of-experiment technique.

Previous Research

Cunnington et al.[2] measured the effective thermal conductivity of seven multilayer insulations at temperatures up to 700 K and at a pressure of 1.33×10^{-3} Pa in 1967. They performed theoretical modeling of the heat transfer using the optically thin approximation for the radiation interchange and compared results with experimental data. DeWitt et al.[3] extended the previous experimental work to 1273 K at a pressure of 0.133 Pa in 1968 and provided a theoretical formulation by neglecting gas conduction and modeling radiation

using the optically thick approximation. Mühlratzer et al.[4] discussed the feasibility of using a metallic thermal protection system with multilayer insulation for hypersonic space transportation in 1989. Keller and his colleagues also provided various theoretical models of heat transfer in multilayer insulation,[5,6] where they neglected solid conduction and used either the optically thick or the modified diffusion approximation for modeling the radiation transfer. Stauffer et al.[7] provided a theoretical formulation of multilayer insulation using the optically thin approximation for the radiation transfer and compared their predictions with previously published experimental results. Siegel modeled the combined solid conduction and radiation heat transfer in thin translucent zirconia ceramic coatings with embedded thin metal foils for application to turbine engine combustors[8] and used the two-flux method for modeling the radiation heat transfer. The thermal design optimization of multilayer insulations has not been addressed in previous research, and the state of the art in multilayer insulation design utilizes uniformly spaced foils evenly distributed throughout the entire insulation thickness.[4]

Description of Multilayer Sample

The multilayer sample investigated in this study for validation of the numerical heat-transfer model consisted of five reflective foils stacked between six layers of alumina fibrous insulation spacers. The gold-coated ceramic reflective foils were $304.8 \times 304.8 \times 0.0404$ mm with a density of 1343 kg/m^3. The fibrous insulation spacers were made of high purity polycrystalline alumina with a density of 24 kg/m^3. The interior four fibrous insulation spacers were 3.83 mm thick, whereas the two outer fibrous insulation spacers were 1.83 mm thick. The insulation sample had an overall height of 19.14 mm with a density of 37.1 kg/m^3.

Thermal Testing Apparatus

Both steady-state and transient tests were used for studying the thermal behavior of multilayer insulations and for validating the numerical heat-transfer model used in the design study. A description of the steady-state and transient thermal testing apparatus is provided.

Steady-State Thermal Testing Apparatus

A thermal conductivity apparatus was developed to measure the steady-state effective thermal conductivity of the multilayer insulation. The apparatus used in this study followed the general guidelines from the American Society for Testing and Materials standards,[9] and a schematic of the apparatus is shown in Fig. 1. The test specimen was located between a 6.4-mm-thick Inconel septum panel and a 25.4-mm-thick water-cooled aluminum plate, both plates having dimensions of 304.8×304.8 mm, and the septum plate was heated by a ceramic radiant heater. Refractory ceramic insulation boards (not shown in Fig. 1) were placed around the apparatus to minimize heat losses. The effective thermal conductivity of the sample was measured with septum panel temperature set at nominal temperatures between 373 and 1273 K and with the water-cooled plate maintained around room temperature. The apparatus was located inside a vacuum chamber, and the environmental pressure was varied between 1.33×10^{-5} and 101.32 kPa. All of the tests were conducted in a gaseous nitrogen environment. The water-cooled plate was instrumented with 9 thin-film heat-flux gauges and 10 type-K thermocouples, and the septum panel was instrumented with 23 metal-sheathed type-K thermocouples. An uncertainty analysis was performed to obtain error estimates for the experimentally determined effective thermal conductivity. The overall uncertainty varied between 7.1–8.3% over the entire range of pressures and temperatures, with an average uncertainty of 7.5%. (Details of the experimental apparatus and uncertainty analysis are provided in Ref. 10.) Measurements on a fumed silica board, Standard Reference Material 1459 from the National Institute of Standard and Technology, at temperatures up to 573 K were within 5.5% of published data.[10] The direction of the applied heating in the experimental setup was opposite the local gravity vector in order to minimize natural convection as a mode of heat transfer.

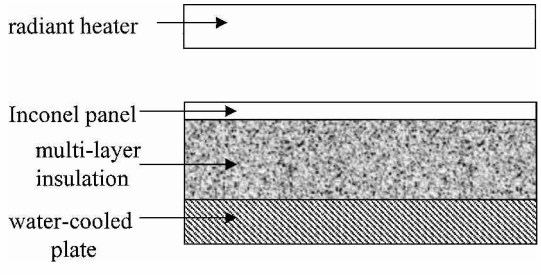

Fig. 1 Schematic of thermal conductivity test apparatus (not to scale).

Transient Thermal Testing Apparatus

A transient thermal test was conducted to simulate reentry aerodynamic heating conditions. The flight trajectory of the NASA winged-body reference vehicle configuration designated 001 (Ref. 11) was used in this study. A plot of the corresponding reentry flight profile is provided in Fig. 2, where the vehicle reentry altitude and velocity variations are shown. The steady-state thermal conductivity apparatus was modified in order to perform the transient thermal test. The heater was changed from a ceramic radiant heater to a quartz lamp radiant heating array in order to be able to provide the rapid transient heating required for simulating the transient reentry heating profile. Furthermore, a 3.2-mm-thick aluminum panel was installed between the Inconel panel and the water-cooled plate. A schematic of the transient thermal test apparatus is shown in Fig. 3. The multilayer insulation was placed between the Inconel and aluminum panels. The Inconel panel served as the hot side solid boundary, whereas the aluminum panel represented the launch vehicle structure. A 13.3-mm-thick alumina fibrous insulation with a density of 24.3 kg/m^3 was placed between the aluminum panel and the water-cooled plate. The Inconel panel's temperature was controlled to simulate the transient radiative equilibrium temperatures[12] corresponding to the reentry flight profile shown in Fig. 2. The water-cooled plate's temperature was maintained around room temperature; therefore, two defined temperature boundary conditions were imposed on the experimental setup, which could also be specified in the numerical heat-transfer model. The pressure in the vacuum chamber was also varied in order to simulate pressures corresponding to the reentry flight profile

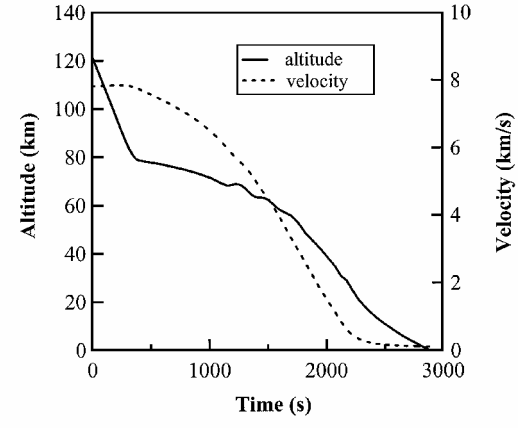

Fig. 2 Reentry flight profile.

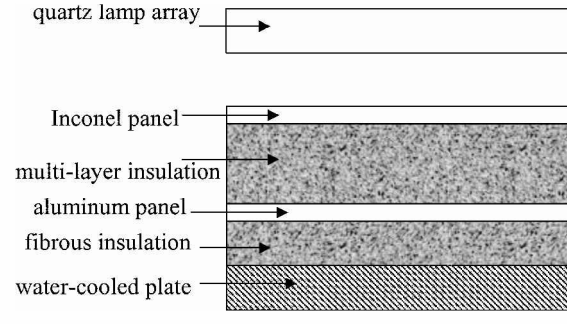

Fig. 3 Schematic of transient thermal test apparatus (not to scale).

shown in Fig. 2. The radiative equilibrium temperature and pressure distribution used in this study corresponded to a location 5.1 m downstream of the nosecap on the centerline of the windward side of the NASA winged-body reference vehicle.[11] The transient thermal test was conducted in a gaseous nitrogen environment. Comparison of predicted and measured temperature of the aluminum panel was used for validation purposes.

Numerical Heat-Transfer Model

The governing conservation of energy equation for the problem of combined radiation and conduction in a radiation participating media bounded by two solid surfaces at specified temperatures is given by[13]

$$\rho c \frac{\partial T}{\partial t} = \frac{\partial}{\partial x}\left(k \frac{\partial T}{\partial x}\right) - \frac{\partial q_r''}{\partial x} \tag{1}$$

subject to the following initial and boundary conditions:

$$T(x, 0) = T_0 \tag{2}$$

$$T(0, t) = T_1(t) \tag{3}$$

$$T(L, t) = T_2(t) \tag{4}$$

Here T_0 is the initial temperature, and T_1 and T_2 are the transient specified temperatures on the boundaries. The gradient of the radiant heat flux is given by[14]

$$\frac{\partial q_r''}{\partial x} = \beta(1 - \omega)(G - 4\sigma T^4) \tag{5}$$

Using the two-flux approximation, the radiant heat flux is related to incident radiation energy per unit area G according to[14]

$$q_r'' = -\frac{1}{3\beta}\frac{\partial G}{\partial x} \tag{6}$$

Therefore, the incident radiation energy per unit area in each fibrous insulation spacer is obtained by solving the following second-order differential equation[14]:

$$-\frac{1}{3\beta^2(1 - \omega)}\frac{\partial^2 G}{\partial x^2} + G = 4\sigma T^4 \tag{7}$$

subject to the following boundary conditions at the bounding surfaces for the fibrous insulation spacers (that is, at two foils or at a foil and a solid bounding surface)[14]:

$$-\frac{2}{3\beta[\varepsilon_i/(2 - \varepsilon_i)]}\frac{\partial G}{\partial x} + G = 4\sigma T_i^4 \tag{8}$$

$$\frac{2}{3\beta[\varepsilon_{i+1}/(2 - \varepsilon_{i+1})]}\frac{\partial G}{\partial x} + G = 4\sigma T_{i+1}^4 \tag{9}$$

where the subscripts i and $i + 1$ refer to the fibrous insulation spacers' two bounding surfaces. The assumptions used in the two-flux formulation consisted of isotropic scattering, homogeneous and gray medium, and diffuse emitting/reflecting surfaces. Although the assumptions of isotropic scattering and gray medium are not valid, they provide simplification of the governing equations to yield an approximate solution.

Gas thermal conductivity does not vary with pressure, but the exchange of heat from gas molecules to bounding solid surfaces is influenced by the environmental pressure in the rarefied and transition flow transport regimes. Thus, an effective gas thermal conductivity was defined as[15]

$$k_g = k_g^* \Big/ \{1 + 2[(2 - \alpha)/\alpha][2\gamma/(\gamma + 1)](1/Pr)(\lambda_m/L_c)\} \tag{10}$$

which relates the effective gas thermal conductivity at various pressures to the gas thermal conductivity at atmospheric pressure k_g^*. The gas molecular mean free path λ_m is given by[16]

$$\lambda_m = \frac{K_B T}{\sqrt{2}\pi d_g^2 P} \tag{11}$$

The characteristic length L_c for gas conduction in fibers having a diameter D_f is defined as[17]

$$L_c = (\pi/4)(D_f/f) \tag{12}$$

The solid fraction ratio f is defined as the ratio of density of fibrous insulation to the density of fiber parent material.

Theoretical modeling of solid conduction through fibers and points of contact between them is difficult, and various empirical relations have been developed to model the solid conduction. The empirical model used in this study was

$$k_s = f^2 k_s^{**} \tag{13}$$

which relates the solid thermal conductivity of fibrous insulation to the thermal conductivity of the fiber parent material (alumina) k_s^{**}. This model is based on the model proposed by Verschoor et al.[17] Although different ways of modeling the interaction between solid and gas conduction have been used by various researchers, in the present study a parallel thermal network model was used for modeling the combined solid and gas conduction in the fibrous insulation[18]:

$$k = f k_s + (1 - f) k_g \tag{14}$$

The finite volume form of the conservation of energy equation [Eq. (1)] was solved using an explicit time-marching formulation. The foils were treated as lumped masses in the numerical model. Constant temperature boundary conditions were used for specifying data from the steady-state thermal conductivity measurements, whereas temporally varying boundary conditions were used for specifying the data from the transient thermal test. Within each fibrous insulation spacer the governing equation and boundary conditions for the incident radiation energy per unit area, given in Eqs. (7–9), were solved using a finite difference technique. Uniform nodal spacing was used in each fibrous insulation spacer region, bounded by either two foils or a foil and a solid bounding surface, whereas the node spacing could vary between regions.

The numerical model using the two-flux formulation was validated with published data[19] for combined conduction/radiation heat transfer in a slab at various values of conduction to radiation ratio parameter and albedo of scattering.[10] The calculated heat fluxes using the numerical model used in the present study were within 1–5% of published data. The numerical model for the combined conduction/radiation heat transfer in the multilayer insulation included 100 nodes, 10 nodes in each of the two outer fibrous insulation spacers, and 20 nodes in each of the four interior fibrous insulation spacers. To study the adequacy of the numerical model mesh, the total number of nodes was doubled. The difference between the effective thermal conductivity predictions for the steady-state tests using 100 and 200 nodes was zero at all pressures except at 0.133 Pa, where effective thermal conductivity differences of 0.0001 W/m/K existed.

Validation of Numerical Model

The specific extinction coefficient and albedo of scattering for the alumina fibrous insulation used in this study were determined in Ref. 10:

$$e = 41.92 + 0.0188\,\mathrm{T} \tag{15}$$

$$\omega = 0.939 + 5.564 \times 10^{-6}\,\mathrm{T} \tag{16}$$

These values were estimated using a genetic algorithm search engine and a least-squares minimization routine based on the difference between measured and predicted effective thermal conductivities of various alumina fibrous insulation samples at a pressure of

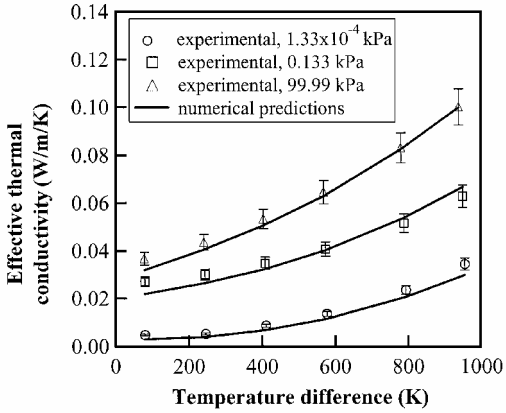

Fig. 4 Comparison of predicted and measured effective thermal conductivity of multilayer insulation.

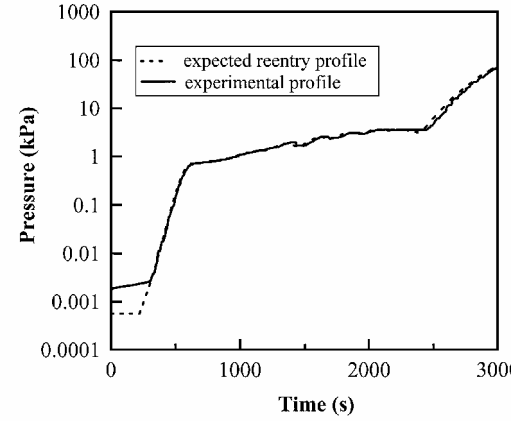

Fig. 5 Comparison of expected flight pressure history with ground-test measured pressure history.

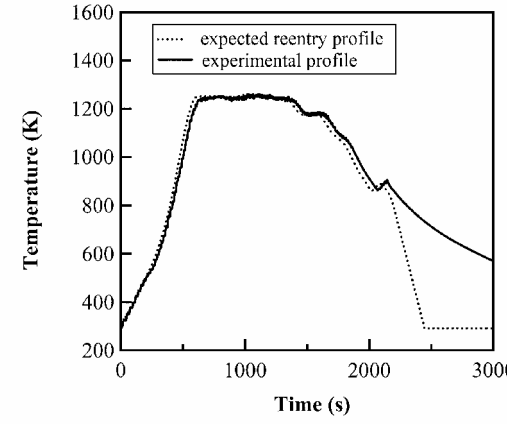

Fig. 6 Comparison of ground-test measured temperature on the Inconel panel with expected reentry radiation equilibrium temperature profile.

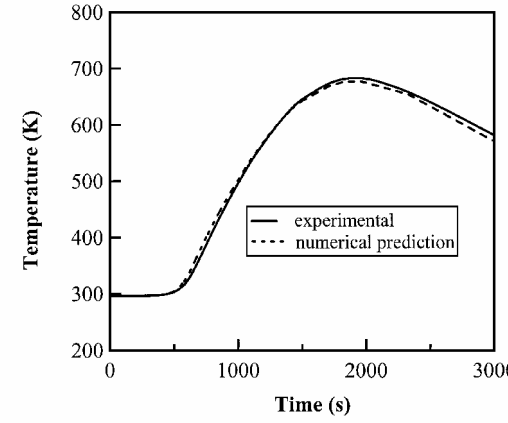

Fig. 7 Comparison of predicted and ground-test measured aluminum panel temperatures for transient multilayer insulation test.

1.33×10^{-2} Pa. The thermal accommodation coefficient for interchange between nitrogen gas and alumina fibers and the reflective foils was determined to be unity.[10] Published data[4] for emittance of the gold-coated foils were used.

Steady-State Results

For validating the numerical model with steady-state thermal conductivity measurements, the numerical solution was marched in time until steady-state conditions were achieved. At steady state the effective thermal conductivity was calculated from the Fourier's law of heat conduction using the calculated total steady-state heat flux (including contributions of both radiative and conductive heat fluxes) and the imposed temperature difference across the medium.

The comparison of predicted and measured effective thermal conductivities for the multilayer sample at nominal pressures of 1.33×10^{-4}, 0.133, and 99.99 kPa is shown in Fig. 4, where the effective thermal conductivity is plotted vs the temperature difference maintained across the sample thickness. The agreement between predictions and measurements at higher pressures and temperature differences larger than or equal to 400 K was within the 7.5% uncertainty range. The agreement was not as good at a pressure of 1.33×10^{-4} kPa. At this pressure the main mechanism for heat transfer was radiation; therefore, the overall numerical predictions were more sensitive to the emittance of gold foils. Differences between predicted and measured effective thermal conductivities for all of the data shown in Fig. 4 averaged 9.8% with a standard deviation of 10.8%. Ignoring the data at 1.33×10^{-4} kPa, the differences averaged 4.6% with a standard deviation of 6.5%. Therefore, the numerical heat-transfer model was validated for steady-state performance of multilayer insulation.

Transient Results

A transient thermal test was conducted with the multilayer insulation sample. The measured temporal variations of the chamber pressure and of the Inconel panel temperature that were achieved in simulating reentry conditions are shown in Figs. 5 and 6, respectively, along with the expected radiation equilibrium temperature and pressure histories corresponding to the reentry flight profile shown in Fig. 2. Data are plotted vs elapsed time from the initiation of atmospheric reentry heating. The measured pressures followed the expected flight pressure profile closely with the exception of elapsed time less than 300 s, where the measured pressures were higher than the expected reentry flight profile pressures. The agreement between the measured temperatures and the expected reentry flight profile temperatures was good until 2300 s, after which the measured temperatures deviated significantly from the expected flight profile. These differences were caused by the high convective cooling rates for the expected flight profile at lower altitudes and subsonic speeds that could not be duplicated in the ground-test vacuum chamber with passive cooling.

In simulating the ground test using the numerical model, the measured temporal variations of the Inconel panel and water-cooled plate temperatures were used for the boundary conditions, and the measured pressure values were used for gas conduction calculations. The predicted and measured aluminum panel temperatures are shown in Fig. 7. The difference between the numerically predicted and ground-test measured temperatures had an average value of 1.8 K, with a standard deviation of 6.5 K, with a maximum difference of 13.2 K. The close agreement between measured and predicted aluminum panel temperatures validated the numerical model for predicting the transient thermal performance of the multilayer insulation subject to conditions similar to expected reentry aerodynamic heating profile.

Design of Multilayer Insulation

The overall goal in insulation design for a reusable launch vehicle is to have the lowest-mass insulation while still protecting the

vehicle's structure from exceeding its design temperature limit during reentry. Recent metallic thermal protection system designs include fibrous insulation[1]; therefore, the multilayer insulation performance was compared with fibrous insulation in a parametric study. A simplified thermal problem simulating reentry aerodynamic heating conditions was used for this comparison. It was assumed that the insulation had a fixed thickness of 76.2 mm, which is representative of a current metallic thermal protection system design,[1] and was located between 3.17-mm-thick Inconel and aluminum panels. It was assumed that the Inconel panel temperature and the environmental pressure varied as the expected reentry profile radiation equilibrium temperature and pressure shown in Figs. 5 and 6, respectively. The aluminum panel was assumed to be adiabatic, a standard assumption for insulation design for space transportation vehicles, even though it has been shown to be very conservative.[20] The insulation function was to prevent the aluminum panel temperature from exceeding a design limit of 450 K. The numerical model described in this article was utilized to model the heat transfer in pure fibrous insulation, and it was found that a fibrous insulation density of 60.48 kg/m^3 was needed in order to not exceed the aluminum panel's design temperature limit. This density resulted in a mass per unit area (product of density and thickness) of 4.61 kg/m^2 for the fibrous insulation sample.

A design-of-experiments approach[21] was used to identify the optimum thermal design for the multilayer insulation. A matrix of design variables was specified. The values of the design variables in each row of the matrix specified an experiment, and the design variables were varied according to an orthogonal array layout.[21] In the present discussion an experiment refers to a numerical solution of the governing heat-transfer equations for the present thermal design problem using the specified design variables of number of reflective foils, spacing between foils, and location of foils in the insulation. Each design variable was investigated at three levels: a high, low, and a nominal estimate. For the number of foils, 2, 4, and 8 were chosen as the low, nominal, and high estimates. Foil spacing design variables chosen were 2, 5, and 8 mm. Foil location was chosen as top, middle, or bottom. For the top design variable condition the foils were located near the hot boundary and the spacing between the top foil and the top of insulation was set equal to the specified foil spacing. For the bottom design variable condition the foils were located near the cold boundary, and the spacing between the lowest foil and the bottom of insulation was set equal to the specified foil spacing. For the middle design variable condition the foils were located symmetrically around the insulation's midplane. The orthogonal array used in this study is shown in Table 1. A full factorial experiment for three parameters at three levels would have required 27 experiments, whereas the use of orthogonal arrays reduced the number of required experiments to nine. The experimental design approach using an orthogonal array assumes that the overall response of the system is obtained by linear superposition of the response of individual design variables with no interaction between the variables.[21] Even though this assumption was not valid for the present design problem, the results illustrated significant trends that could be used in optimum multilayer insulation design.

The transient thermal problem was solved numerically using the design variable settings for each of the nine experiments defined in Table 1. The thickness of the fibrous insulation spacers was adjusted so that the overall thickness of the foils and spacers was held constant at 76.2 mm. For each experimental condition the density of the spacers was chosen uniformly for all of the spacers, and the governing heat-transfer equations were solved numerically to obtain the temperatures on the aluminum panel, which was representative of the launch vehicle structure. A secant search method[22] was used to determine the required density of the fibrous insulation spacers in order to satisfy the constraint of limiting the aluminum panel's maximum temperature to 450 K. The resulting mass per unit area of the nine configurations is listed in Table 1. The relative mass per unit area savings for each configuration was determined by comparison with the mass per unit area of the pure fibrous insulation configuration (4.61 kg/m^2). A negative number for the mass per unit area saving indicates that the mass of the multilayer insulation configuration was higher than the original fibrous insulation. All of the multilayer configurations with foils located at the bottom of the insulation package (near the cold boundary) performed worse than the pure fibrous insulation configuration irrespective of the number foils and foil spacing used. Not only did these designs not improve performance, but foils at these locations could not even thermally compensate for the removal of the equivalent mass of fibrous insulation. The multilayer configurations with the foils located at the top (near the hot boundary), trial numbers 1, 6, and 8, had the best performance. The multilayer configurations with the foils spaced in the middle of the insulation thickness (trials 2, 4, and 9) produced better results compared to fibrous insulation but did not match the performance of designs with foils located near the hot boundary. The best result for multilayer configurations with middle foil locations was obtained with trial 9, resulting in mass saving of 2.2%. This configuration had eight foils with 8 mm spacing and was nearly a design with foils uniformly spaced throughout the insulation thickness. (The top and bottom spacer regions were 9.9 mm thick, and the seven interior spacers were 8 mm thick.) But its performance was not as good as trial 8, which had the same number of foils (eight) located near the hot boundary with 5-mm foil spacing (6.7% mass saving). Analysis of variance[21] was used to investigate the effect of each of the design variables on the insulation mass, and it was found that the foil location was the dominant variable.[10]

Table 1 Results of design-of-experiment analysis

Trial number	Number of foils	Foil spacing, mm	Foil location	Mass/area, kg/m^2	Mass/area saving,[a] %
1	2	2	Top	4.43	3.8
2	2	5	Middle	4.60	0.3
3	2	8	Bottom	4.61	−0.1
4	4	2	Middle	4.56	0.9
5	4	5	Bottom	4.64	−0.7
6	4	8	Top	4.50	2.4
7	8	2	Bottom	4.70	−1.9
8	8	5	Top	4.30	6.7
9	8	8	Middle	4.51	2.2

[a]A negative number indicates mass gain compared to fibrous insulation.

To further investigate foil spacing, an additional experiment was performed similar to trial 1, with two foils with a foil spacing of 5 mm. The resulting mass saving was 2.9%, which was not as good as the mass saving of 3.8% obtained in trial 1 with two foils with a foil spacing of 2 mm. This proved that using the lowest possible foil spacing (2 mm) with the foils located near the hot boundary is the optimum multilayer design philosophy.

These results are consistent with basic heat-transfer principles. The reflective foils' main function is to provide high thermal resistance to radiation heat transfer in the insulation because of their high reflectance. The resistance value is inversely proportional to the optical thickness of the fibrous insulation spacers between the foils. If the fibrous insulation spacer is optically thick, the reflectance of the foils will not have any appreciable effect on the overall radiation heat transfer.[13] The fibrous insulation spacer should have a low value of optical thickness so that the high reflectance of its bounding surfaces (foils) can influence the radiation heat transfer. The optical thickness of the fibrous insulation spacer is the product of the spacer thickness, density, and specific extinction coefficient according to[23]

$$\tau_o = L'\rho e \tag{17}$$

Because the specific extinction coefficient is an intrinsic property of the spacer material, spacer thickness and density are the only variables that can affect the optical thickness. For a fixed spacer density lowering the spacer thickness results in a lower optical thickness and a higher thermal resistance to radiation heat transfer. A foil spacing of 2 mm was the lowest reasonable spacer thickness that could be easily achieved on a consistent basis. Furthermore, because radiation is the dominant mode of heat transfer near the hot boundary[10] placing the foils in this region will impede radiation heat transfer more effectively.

Using the optimum design philosophy of foil spacing of 2 mm with the foils stacked near the hot boundary, the influence of the number of foils was investigated. Results were obtained with 1, 2, 4, 8, and 16 foils and are presented in Table 2. With 16 foils the

Table 2 Mass savings for optimized multilayer insulation configurations compared to fibrous insulation

Number of foils	Mass/area saving, %	Mass/area saving per foil, %/foil
1	2.9	2.9
2	3.8	1.9
4	7.2	1.8
8	12.6	1.6
16	22.2	1.4

bottom spacer is 43.5 mm thick, and so all of the foils are located in the upper half of the insulation thickness. One foil resulted in a mass saving of 2.9%. The mass saving increased with increasing number of foils, reaching 22.2% for 16 foils. The mass saving per foil is also listed in the table. The largest mass saving per foil was achieved with one foil (2.9% per foil), and the saving per foil decreased with increasing foil number.

Conclusions

A numerical model was developed for modeling combined radiation/conduction heat transfer in high-temperature multilayer insulations. The numerical model was validated by comparison with steady-state effective thermal conductivity measurements and by transient thermal tests simulating reentry aerodynamic heating conditions. A design-of-experiment approach was used to determine the optimum design for multilayer insulations subjected to reentry aerodynamic heating conditions. It was found that use of 2-mm foil spacing and locating the foils near the hot boundary with the top foil 2 mm away from the hot boundary resulted in the most effective insulation design. For the specific conditions investigated, a 76.2-mm-thick multilayer insulation using 1, 4, or 16 foils resulted in 2.9, 7.2, or 22.2% mass per unit area savings, respectively, compared to a fibrous insulation sample at the same thickness.

Acknowledgments

The author would like to thank the following NASA Langley Research Center employees for their invaluable support: Wayne D. Geouge for fabrication and instrumentation of the test apparatus and Jeffrey R. Knutson for providing temperature and pressure controls for the tests. The author would also like to express his gratitude to Karin Handrick, MAN Technologie AG, and Steve D. Miller, S. D. Miller & Associates, for providing various multilayer insulation samples.

References

[1]Blosser, M. L., Chen, R. R., Schmidt, I. H., Dorsey, J. T., Poteet, C. C., and Bird, R. K., "Advanced Metallic Thermal Protection System Development," AIAA Paper 2002-0504, Jan. 2002.

[2]Cunnington, G. R., Zierman, C. A., Funai, A., and Lindahn, A., "Performance of Multilayer Insulation Systems for Temperatures to 700K," NASA CR-907, Oct. 1967.

[3]DeWitt, W. D., Gibbon, R. L., and Reid, R. L., "Multi-Foil Type Thermal Insulation," *Intersociety Energy Conversion Engineering Conference Record*, Inst. of Electrical and Electronics Engineers, New York, 1968, pp. 263–271.

[4]Mühlratzer, A., Handrick, K., and Weber, K.-H., "Hermes Thermal Protection System Internal Multilayer Insulation (IMI)," International Astronautical Federation, Paper 90-282, Oct. 1990.

[5]Keller, K., Blumenberg, J., and Tomsik, J., "Fibre Orientation and the Conduction of Heat by a Gas Enclosed in Ceramic Layers," *Journal of Flight Sciences and Space Research*, Vol. 12, No. 4, 1988, pp. 258–260.

[6]Keller, K., Hoffmann, M., Zörner, W., and Blumenberg, J., "Application of High Temperature Multilayer Insulations," *Acta Astronautica*, Vol. 26, No. 6, 1992, pp. 451–458.

[7]Stauffer, T., Jog, M., and Ayyaswamy, P., "The Effective Thermal Conductivity of Multi Foil Insulation as a Function of Temperature and Pressure," AIAA Paper 92-2939, July 1992.

[8]Siegel, R., "Transient Thermal Analysis for Heating a Translucent Wall with Opaque Radiation Barriers," *Journal of Thermophysics and Heat Transfer*, Vol. 13, No. 3, 1999, pp. 277–284.

[9]"Standard Test Method for Thermal Conductivity of Refractories," *Annual Book of ASTM Standards*, Vol. 15.01, American Society for Testing and Materials, West Conshohocken, PA, 2000, pp. 54–59.

[10]Daryabeigi, K., "Design of High Temperature Multi-Layer Insulation," Ph.D. Dissertation, Mechanical and Aerospace Engineering Dept., Univ. of Virginia, Charlottesville, VA, May 2000.

[11]*Access to Space Study-Advanced Technology Team (Option 3). Vol. III, Design Handbook*, NASA, Washington, DC, July 1993.

[12]Thornton, E. A., *Thermal Structures for Aerospace Applications*, AIAA, Reston, VA, 1996, p. 18.

[13]Sparrow, E. M., and Cess, R. D., *Radiation Heat Transfer* (augmented ed.), McGraw–Hill, New York, 1978, pp. 255–271.

[14]Özişik, M. N., *Radiative Transfer and Interactions with Conduction and Convection*, Wiley, New York, 1973, pp. 327–343.

[15]Gebhart, B., *Heat Conduction and Mass Diffusion*, McGraw–Hill, New York, 1993, pp. 442–444.

[16]Williams, S. D., and Curry, D. M., "Predictions of Rigid Silica Based Insulation Conductivity," NASA TP-3276, Jan. 1993.

[17]Verschoor, J. D., Greebler, P., and Manville, N. J., "Heat Transfer by Gas Conduction and Radiation in Fibrous Insulation," *Journal of Heat Transfer*, Vol. 74, No. 8, 1952, pp. 961–968.

[18]Schneider, P. J., "Conduction," *Handbook of Heat Transfer*, edited by W. M. Rohsenow and J. P. Hartnet, McGraw–Hill, New York, 1973, Chap. 3, p. 122.

[19]Özişik, M. N., *Radiative Transfer and Interactions with Conduction and Convection*, Wiley, New York, 1973, pp. 470–472.

[20]Ko, W. L., Quinn, R. D., and Gong, L., "Finite-Element Reentry Heat-Transfer Analysis of Space Shuttle Orbiter," NASA TP 2657, Dec. 1986.

[21]Phadke, M. S., *Quality Engineering Using Robust Design*, Prentice–Hall, Englewood Cliffs, NJ, 1989, pp. 41–65.

[22]Gerald, C. F., and Wheatley, P. O., *Applied Numerical Analysis*, 5th ed., Addison Wesley Longman, Reading, MA, 1994, pp. 35–37.

[23]Siegel, R., and Howell, J. R., *Thermal Radiation Heat Transfer*, 2nd ed., 1981, McGraw–Hill, New York, 1981, pp. 426, 427.

M. Torres
Associate Editor